

Uniform Single-Sided Induction Heating Using Multiphase, Multi-Resonant Halbach Windings

Arijit Banerjee, Al-Thaddeus Avestruz, Kawin Surakitbovorn, Arthur H. Chang, and Steven B. Leeb
Department of Electrical Engineering and Computer Science, Massachusetts Institute of Technology
Cambridge, Massachusetts, USA

Abstract—Traditional induction heating cooktops typically employ a circular planar coil in resonance excited by a switching inverter. This configuration results in stray magnetic fields below the coil and non-uniform heating profile on the top. This paper presents the concept of multiphase, multi-resonant induction heating using a Halbach winding arrangement to eliminate the shortcomings of the traditional cooktop. A multiphase winding structure enables a traveling magnetic field at the target, which results in uniform heating profile. Operating the phases at different resonances deliver power at different frequencies. The winding and drive structure developed in this paper can be applied to many other applications, including chargers and wireless power delivery systems.

I. INTRODUCTION

Induction heating is widely used for industrial [1], medical [2, 3], and consumer [4, 5] applications. Cooktop induction heaters often consist of circular, planar, multiturn coils excited with resonant power electronic circuits operating in the range of tens to hundreds of kHz [5]. This arrangement has considerable stray magnetic fields at the bottom of the coil and also results in non-uniform heating along the surface of the target. Mitigation of these consequences has been addressed individually using multiphase windings [6], ferrite planes [7], optimized shielding [8], and even zone controlled induction heating [9, 10]. These solutions may not only increase the cost, weight, size, and complexity of the control, but also lead to susceptibility to mechanical failures. Reference [11] developed a single-phase Halbach winding concept for induction heating to achieve an essentially unidirectional magnetic field by significantly reducing the stray magnetic field on the underside of the coil. The three-layer winding structure emulates a Halbach array where magnets are replaced with ac current coils. The single-phase winding arrangement, heats the target with a sinusoidal heating profile as expected from a Halbach array.

This paper presents a Halbach winding arrangement based on maximizing the ratio of energy distribution on the top compared to the bottom for a given winding configuration. The investigation leads to an optimized Halbach winding with only two layers of conductors. Further, a second two-layered Halbach winding can be superimposed that is

spatially orthogonal to the original winding to create a multiphase Halbach winding arrangement. Ideally the two windings are decoupled by the spatial arrangement; using currents that are temporally orthogonal leads to a traveling magnetic field, resulting in uniform heating. Temporal orthogonality is typically implemented by exciting two currents at the same frequency but 90° out of phase. In practice, a small coupling between the windings exists because of finite tolerances. This leads to difficulty in simultaneously maintaining the phase orthogonality and controlling the individual current magnitudes. By using two different frequencies, both temporal orthogonality and independent magnitude control can be achieved, enabling a uniform heating profile. An 8 inch x 15 inch prototype designed with the proposed concept is used to demonstrate uniform single sided induction heating along with the associated resonant circuits.

II. MULTIPHASE HALBACH WINDING DESIGN

Halbach arrangements of permanent magnets have been used in the rotors of permanent magnet motors [12]. These Halbach arrangements are attractive because the back iron of the electrical motor can be eliminated reducing mass and inertia. For induction heating applications, such as an induction cooktop, where only one sided heating is necessary, a Halbach arrangement can significantly reduce the need for magnetic shields at the bottom, which typically consist of ferrites and conductor plates. The magnetic field in the induction cooktop needs to be time-varying to induce current on the target for Joule heating. This requires windings that carry time-varying currents placed so that a magnetic field is produced only on a single side.

The following section discusses the design of a winding arrangement that can emulate a Halbach array so that the magnetic field on the top is much greater than the bottom. The design is based on a four-step process. First, the magnetic field and the stored energy are calculated in different sections for an arbitrary arrangement of conductors in an enclosed volume. Second, the conductor ampere-turns and locations are optimized so that the magnetic energy on the top dominates.

Third, the effect of introducing highly permeable materials at the top and bottom of the optimized conductor arrangement is investigated using a finite element simulation. Finally the conductors are connected so that the appropriate current polarities form a Halbach winding array.

A. Stored Energy in the Magnetic Field for an Arbitrary Conductor Arrangement

An arbitrary conductor arrangement ($C_1, C_2, C_3, \dots, C_k$) is considered within a rectangle $ABCD$ of length L and height h as shown in Fig. 1. In a three-dimensional coordinate frame, the rectangle is assumed to have unity dimension in the z -direction. The conductors carry different amp-turns (ATs), either positive or negative, along the z -direction. The magnetic field at a distance (x,y) due to each of these conductors can be calculated from Ampere's Law. Assuming that the magnetic field has no variation along the z -direction, the net magnetic field at (x,y) due to the complete arrangement can be calculated by superposition and is given by,

$$\begin{aligned} H_{x,net} &= -\sum_{i=1}^K \frac{c_i (y - y_i)}{2\pi [(x - x_i)^2 + (y - y_i)^2]} \\ H_{y,net} &= \sum_{i=1}^K \frac{c_i (x - x_i)}{2\pi [(x - x_i)^2 + (y - y_i)^2]} \\ \vec{H}_{net} &= H_{x,net} \hat{x} + H_{y,net} \hat{y} \end{aligned} \quad (1)$$

To emulate a Halbach array, the energy stored on the top section of the conductor arrangement, represented as $ABEF$ in Fig. 1 must be significantly greater than the energy stored in the bottom section, represented as $DCHG$. Assuming that the conductor arrangement is periodic along the x -direction with periodicity of length L but with alternating polarity of ATs, the boundary condition along 'EH' and 'FG' can be applied as,

$$\begin{aligned} H_{x,EH} &= H_{x,FG} = 0 \\ H_{y,EH} &= -H_{y,FG} \end{aligned} \quad (2)$$

Assuming $EFGH$ is free space, the stored energy in the three sections, top $ABEF$, middle $ABCD$ and bottom $DCGH$, are

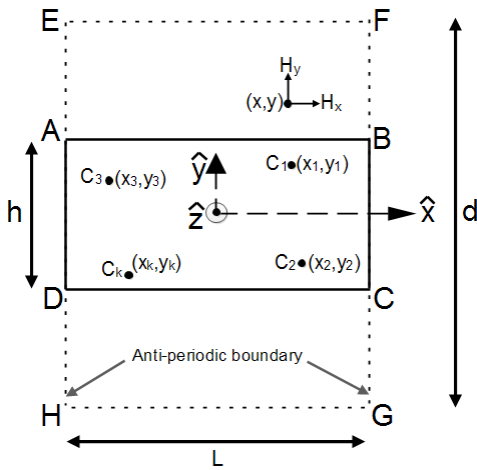


Figure 1. Arbitrary arrangement of conductors carrying current in z -direction in an enclosed area $ABCD$.

given by,

$$\begin{aligned} E_{top} &= \frac{\mu_0}{2} \int_{-L/2}^{L/2} \int_{h/2}^{d/2} H_{net}^2 dy dx \\ E_{bottom} &= \frac{\mu_0}{2} \int_{-L/2}^{L/2} \int_{-h/2}^{-d/2} H_{net}^2 dy dx \\ E_{middle} &= \frac{\mu_0}{2} \int_{-L/2}^{L/2} \int_{-h/2}^{h/2} H_{net}^2 dy dx \end{aligned} \quad (3)$$

B. Optimization of Conductor Arrangement Using a Genetic Algorithm

The design goal is to optimize the conductor locations (x_k, y_k) and the ampere-turns C_k of the K conductors in $ABCD$ to maximize the ratio of the magnetic field at the top to the magnetic field at the bottom. Quantitatively, the directional property can be expressed by a parameter Γ , the *Directivity*, which is defined as the ratio of total magnetic energy on the top to the total magnetic energy in the bottom,

$$\Gamma = \frac{E_{top}}{E_{bottom}} \quad (4)$$

Additionally, the effectiveness of the conductors in transferring energy to the top relative to the energy stored in the middle and the bottom can be indirectly measured using the parameter Λ , the *Effectivity*. This is defined as the ratio of total magnetic energy on top to the sum of the total energies stored in the middle and bottom,

$$\Lambda = \frac{E_{top}}{E_{bottom} + E_{middle}} \quad (5)$$

The inverse product of Γ and Λ is used as the cost function for the conductor arrangement optimization. Based on reducing the complexity of the final winding structure and the spatial harmonic content of the magnetic field, three constraints are placed on x_k, y_k and C_k . First, constraining y_k between two discrete levels $+h/2$ and $-h/2$ enforces two layers of conductors to synthesize the winding pattern. This minimizes the amount of copper required, as well as the cost of manufacturing for the overall winding. However, h is a free optimization variable that determines the distance between the two layers. Second, constraining C_k to only signed integer values (Z) allows the use of a single continuous wire for constructing the winding. Finally, symmetry across the y -axis, shown in Fig.1, is imposed to eliminate the even harmonics in the spatial distribution of the magnetic field. That is, if a conductor is placed at (x_k, y_k) carrying the C_k AT, there must be another conductor placed at $(-x_k, y_k)$ carrying equal AT. The symmetry requirement enforces bounds on x_k between origin and half of the length. The complete optimization problem is,

$$\min_{x_i, y_i, C_i, h} S = \frac{1}{\Gamma \Lambda}$$

Subject to:

$$\begin{aligned}
|x_i| &< L/2 \\
y_i &\in \left[-\frac{h}{2}, \frac{h}{2}\right] \\
C_i &\in Z \\
(-x_{i+(K/2)}, y_{i+(K/2)}, C_{i+(K/2)}) &= (x_i, y_i, C_i) \\
i &\leq \frac{K}{2}
\end{aligned} \tag{6}$$

Table I summarizes the actual values chosen for the different variables for an exemplary design of a Halbach conductor arrangement using six total conductors. The optimization is run in MATLAB using the Genetic Algorithm in the Optimization Toolbox. For ease of numerical integration to evaluate stored energy in different sections using (3), the bounds on the integral are chosen such that they do not enclose the conductors.

TABLE I. OPTIMIZATION FOR AN EXEMPLARY DESIGN: PARAMETERS AND VARIABLE BOUNDS

Parameters	Values	
L	1.2 inch	
K	6	
d	12 inch	
Variables	Lower Bound	Upper Bound
h	0.05 inch	0.4 inch
Z	-1	1

Figure 2 shows the optimized conductor placement and ATs generated by the genetic algorithm based on the parameters and constraints. The magnitude of the magnetic field, H for the optimized conductor arrangement is calculated using (2). The near-sinusoidal variation of the magnitude along x -direction at a certain distance away from the top layer is shown in Fig. 3. As expected, the magnitude decreases with an increase in distance in the y -direction. Figure 4 shows the variation of magnitude of the magnetic field as a function of distance along y -direction at $x=0$. The dashed lines demarcate the location of the top conductor layer and the bottom conductor layer. As expected, the bottom conductor layer drastically improves the roll off of the magnetic field at the bottom so that it is negligible at 0.5 inches away. It is clear that this effect is not due to the distance as the absence of the bottom conductor layer increases the magnetic field in the bottom. A less significant impact from the bottom conductor layer can be observed on the top side magnetic field. The

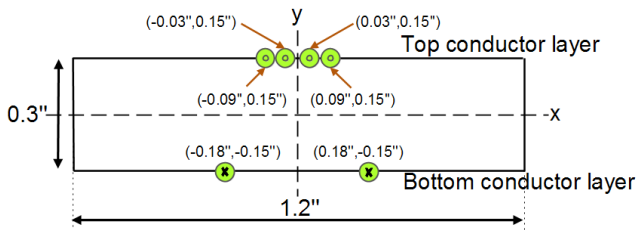


Figure 2. Optimized Halbach cell with six conductors for the chosen parameter and geometry bounds.

magnetic field pattern as shown in Fig. 3 and Fig. 4 closely resembles the field pattern from an ideal Halbach array [13].

So far the computation of the energy and the optimization has been based on the assumption that the conductors are in free space and without any permeable material (target) in proximity. A static finite element analysis is performed in COMSOL to evaluate the presence of a highly permeable material in proximity to the optimized Halbach cell. Figure 5 shows the flux density distribution when two highly permeable (steel) targets are placed equidistantly from the top conductor layer. Without energizing the bottom conductors, equal flux density is observed on both of the targets, as expected. The excitation of the second layer cancels much of the field on the bottom compared to the top. The conductors between the adjacent cells, when connected together with the correct current polarity, form a single phase winding with multiple cells behaving together to form a complete Halbach array.

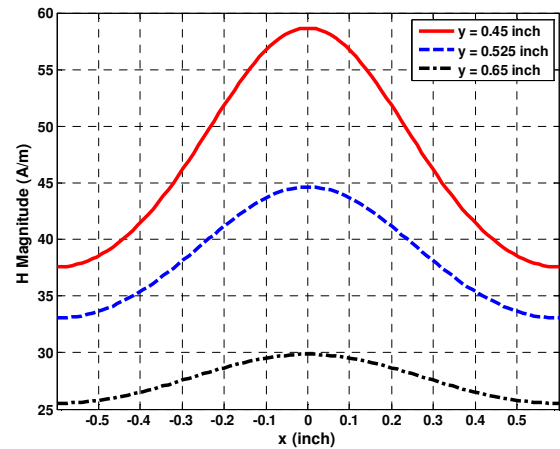


Figure 3. Near-sinusoidal variation of the magnetic field along x -direction for the optimized Halbach conductor arrangement using six conductors.

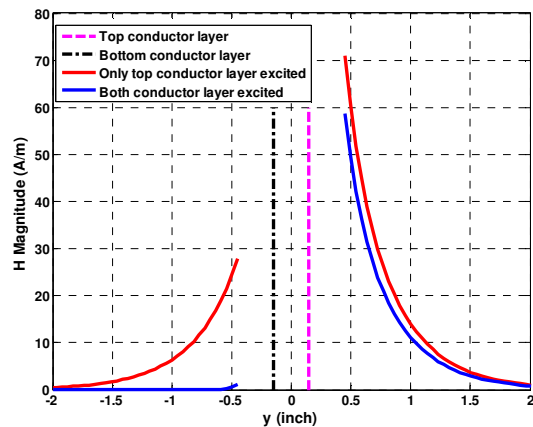


Figure 4. Rapid roll-off of the magnetic field on the bottom of the cell compared to the top in the presence of the bottom conductor layer at $x=0$.

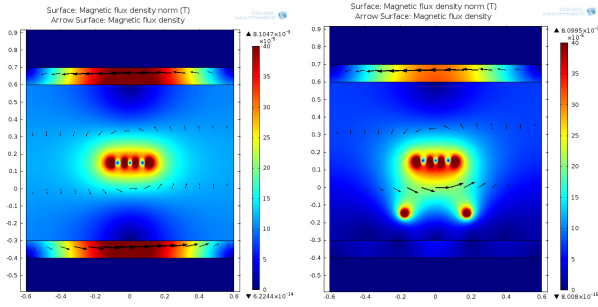


Figure 5. Finite element analysis using COMSOL to evaluate presence of highly permeable target on the top and the bottom, 0.5 inch equidistant from the top winding layer. (a) Equal flux density on the top and bottom permeable material with unexcited bottom conductor layer. (b) Higher flux density on the top compared to bottom with excitation enabled in the bottom conductor layer.

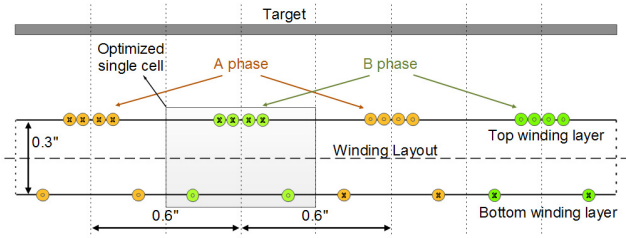


Figure 6. Two-phase winding layout using optimized Halbach conductor arrangement such that the windings are orthogonal in space to enable uniform heating of the target when placed on top.

C. Realization of Two-Phase Halbach winding for Uniform Heating

The single-phase Halbach winding designed in the previous section is able to produce directional magnetic fields. However, the magnetic field has a near-sinusoidal variation along x-direction on the top as seen in Fig. 3. This results in a pulsating magnetic field of varying magnitude along the x-direction when the winding is excited with time-varying current. This creates a non-uniform heating pattern on the target.

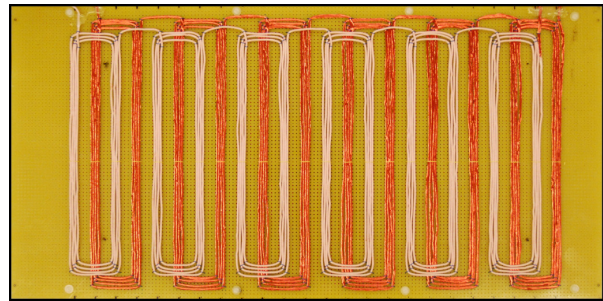
Non-uniformity in heating can be mitigated by using multiple spatial phases of Halbach windings. In the example winding design, a two-phase winding structure is created by interleaving two sets of the Halbach windings such that they are spatially orthogonal, i.e. the flux from one of the phase windings ideally does not couple with the other phase winding. The two-phase windings layout and dimensions are shown in Fig. 6.

The example winding layout is based on Fig. 6 constructed using Litz wire (175 strands x 40 ga) on an 8.5" x 17" G-10 board. Twelve optimized cells are used for each phase as shown in Fig. 7 to obtain a demonstrable length of uniform heating. The served Litz wire (seen as white) forms the A-phase winding while the unserved one (seen as red) forms the B-phase winding. Kevlar thread is used to keep the Litz wire in place on the G-10 board. Figure 7(a) shows the

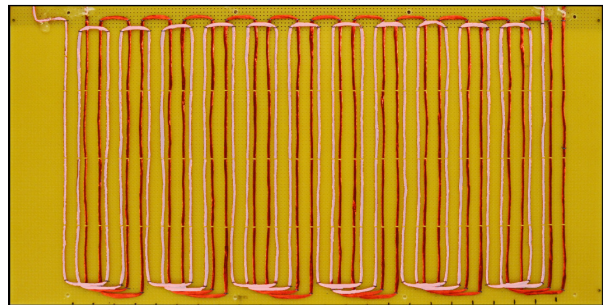
top winding layer of the two phases and 7(b) shows the bottom winding layer of two phases. The two winding layers are assembled with a gap of 0.3 inch as shown in Fig. 7(c). A steel target is shown on the top of the winding at a distance of 3/8th inch above the top layer.

III. WINDING EXCITATION USING RESONANT INVERTER

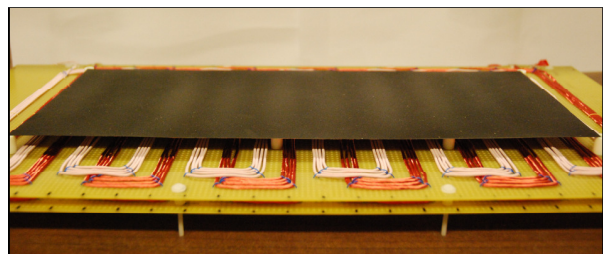
A series resonant circuit operating at hundreds of kHz can excite the currents in an induction heating coil. The proposed two-phase (A & B) winding structure requires two resonant circuits to excite the individual phases such that the currents in the two phases are orthogonal in time. A simple approach for realizing temporally orthogonal currents in two phases is to drive the phases at same frequency but one with a sine and the other with a cosine excitation. However, because of practical winding imperfections, there is mutual coupling between the two phases, i.e. current is induced in the B-phase even when only the A-phase is energized and vice versa. The mutual coupling makes it challenging to have independent excitation control for each of the phases. Therefore, the two



(a)



(b)



(c)

Figure 7. Prototype of the optimized two phase Halbach winding: white—Phase A and red—Phase B. (a) Top winding layer (b) Bottom winding layer (c) Assembled winding structure with steel target on top.

phases are designed to resonate at two different frequencies where the separation in tuning attenuates the effect of mutual coupling. The time orthogonality of the excitation currents is achieved on a time-averaged basis. Since the heating of the target is based on the average power dissipation, the overall excitation for the two phases at different frequencies produces uniform heating.

This section discusses the multi-resonant circuit used to drive the two phases of the winding structure. An ac analysis is performed in a lumped parameter SPICE model showing the effect of mutual coupling between the two phases when either phase is excited individually. The SPICE model will also be used to show the benefit of exciting the two phases with different frequencies even in the presence of mutual coupling. Finally, an average power transfer model is used to derive the heating pattern on the target based on the magnetic field when the individual phases are excited with different frequencies. The analytical formulation shows that the average power transfer to the target is position independent along x-direction.

A. Multi-Resonant Excitation of the Two-phase Winding

Tuning the excitations for the resonances of the two phases, requires measuring the terminal impedances of the prototype winding. The parameters are measured using an impedance analyzer. The measured inductance of the A-phase is 16.12 μH while the measured inductance of the B-phase is 16.85 μH . Additionally, the measured mutual inductance between the two phases is 0.71 μH . Based on these measurements, the coupling coefficient k is calculated to be only 4%.

To evaluate the effect of even a weak mutual coupling between the two phases on resonant excitation, a simplified lumped model of the prototype winding is used in SPICE as shown in Fig. 8. For simplicity, the distributed capacitive coupling between the two phase windings, is modeled by a single lumped capacitor C_c in this model. The windings are individually connected to two resonant capacitors C_{r1} and C_{r2} to form the series resonant circuits. An ac sweep is performed on the A-phase with the B-phase shorted, which is the Thevenin equivalent of a voltage source inverter. First equal resonant capacitors for the both phases is examined. For example, with $C_{r1} = C_{r2} = 10$ nF; Fig. 9 (top plot) shows the current response in the A and B phases. As expected, the A-phase resonates at 400 kHz, however, significant circulating current is induced in the B-phase at the same frequency due to the mutual coupling. This shows that the A and B-phases cannot be driven independently using two separate voltage sources making it challenging to achieve temporal orthogonality in the phase excitation currents.

However, the cross coupling in the two phase currents can be significantly minimized provided the two phases are tuned to two different frequencies. For example, choosing C_{r1} to be 20 nF while keeping C_{r2} at 10 nF, as shown in Fig. 8, decouples the resonances between the two phases. With the A-phase resonating at 280 kHz, the impact observed in the B-phase due to the A-phase is negligible, as shown in Fig. 9 (bottom plot). A symmetrical analysis using ac sweep on B phase with shorted A phase leads to an identical conclusion

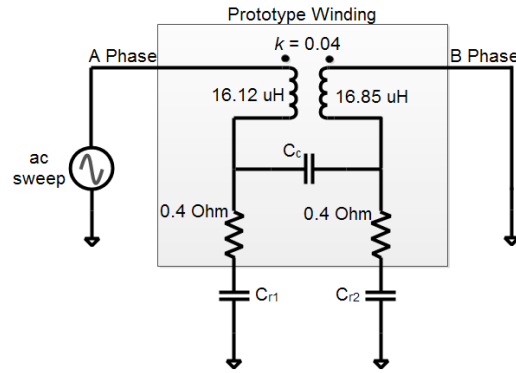


Figure 8. Simplified SPICE model to evaluate the effect of stray coupling between the two phases. An ac sweep is performed in A phase with shorted B phase.

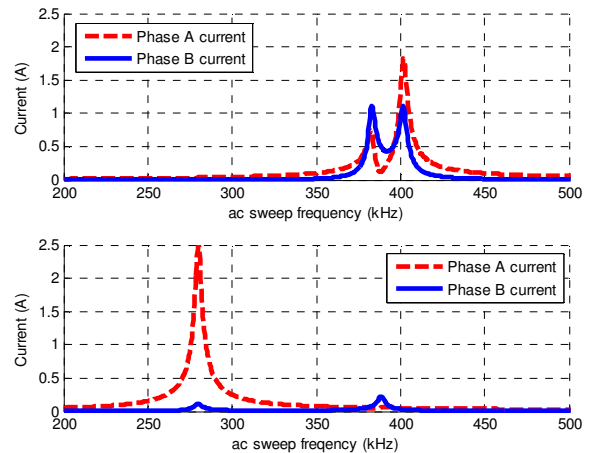


Figure 9. SPICE ac sweep result: Effect of stray coupling on B-phase with only A-phase excited. Top: Both phases tuned at 400 kHz. Significant current induced in the B-phase at same frequency. Bottom: A-Phase is tuned at 280 kHz while B-phase is tuned at 387 kHz. Cross-coupling effect is significantly reduced.

that the multi-resonant excitation of the two phases provides independent control of the phase currents. The multi-resonant power circuit used to excite the two phases for the prototype winding is shown in Fig. 10.

B. Average Power Transfer to the Target with Two Phase Winding Excited at Different Frequencies

The multi-resonant excitation reduces the effect of stray coupling between the two phase windings enabling independent control of the two phases. However, the excitation directly impacts the instantaneous magnetic field produced by the individual windings. So it is worthwhile to investigate this effect on the heating pattern at the target. For example, the magnetic flux density of the fundamental spatial frequency of the A-phase at a point y above and x along a Halbach surface with height h can be shown as in [10],

$$B_A = \mu_0 \alpha k N (1 - e^{-kh}) e^{-ky} I_A \cos kx \quad (7)$$

Where $k = 2\pi / \lambda$ is the radian reciprocal of the array wavelength or pole pitch, N is the equivalent number of turns, I_A is the current excitation in the A-phase, and α is a

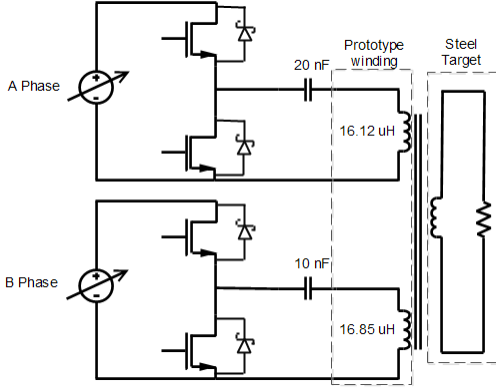


Figure 10. Two independent resonant power circuits are used to drive the prototype two-phase Halbach windings. Phase A tuned resonant frequency is 280 kHz and Phase B tuned resonant frequency is 387 kHz.

geometric factor. Due to the orthogonal placement of the B-phase winding relative to the A-phase, the magnetic flux density of the B phase can be expressed as,

$$B_B = -\mu_0 \alpha k N (1 - e^{-kh}) e^{-ky} I_B \sin kx \quad (8)$$

Assuming the windings are identical and with individually controllable phase currents, the total magnetic flux density can be written by superposition as

$$B_T = \mu_0 \alpha k N (1 - e^{-kh}) e^{-ky} [-I_B \sin kx + I_A \cos kx] \quad (9)$$

The changing magnetic field due to the time-varying current excitations as computed above will result in eddy currents in the target and thereby dissipate power and heat the target. The power dissipated on the target is proportional to the square of the flux density. Thus, the instantaneous power delivered to the coil can be equivalently written as,

$$P_{T_{\text{arget}}} = K_B I_B^2 \sin^2 kx + K_A I_A^2 \cos^2 kx - K_B K_A I_B I_A \sin kx \cos kx \quad (10)$$

The terms K_A and K_B takes into account the difference in skin depths for the target at different excitation frequencies. Assuming that the current excitation in the A-phase has frequency ω_1 and the current excitation in the B-phase has frequency ω_2 , the average power transferred to the target can be calculated as,

$$\begin{aligned} \langle P_{T_{\text{arget}}} \rangle &= \frac{K_B}{2} |I_B|^2 (1 - \cos 2kx) + \frac{K_A}{2} |I_A|^2 (1 + \cos 2kx) \\ &\quad - \frac{K_A K_B}{4} \langle I_B I_A \rangle \sin 2kx \end{aligned} \quad (11)$$

Assuming that equal power is transferred from the two phases to the target and because of the orthogonality of sinusoids with different frequencies, the average power can be simplified to,

$$\langle P_{T_{\text{arget}}} \rangle = \frac{K_A}{2} |I_A|^2 + \frac{K_B}{2} |I_B|^2 \quad (12)$$

The average power transferred to the target is uniform along the x-direction enabling uniform heating on the target.

IV. EXPERIMENTAL RESULTS

The prototype winding is tested with two different experiments to verify the directionality of the magnetic field produced by the windings and the uniformity of heating that can be achieved using the two phases when excited with the two resonant power circuits. The target used is made of steel of thickness 5 mil and of dimension 12 inch by 7 inch.

A. Change in Effective Resistance of the Winding Due to the Proximity of the Target

The prototype winding as shown in Fig. 7 is tested for performance in terms of directionality using an impedance analyzer. The resistance of the A-phase winding is measured as a function of excitation frequency and plotted in Fig. 11. The change in the terminal resistance of the two-layer A-phase winding is much higher when the target is above than an equidistant 0.5 inch below. The difference in the loading effect shows strongly asymmetric magnetic coupling to the target between the top and the bottom, which is expected from a Halbach winding.

B. Thermal Performance of the Proposed Induction Heater

The prototype windings are excited using two resonant inverters with the steel target at 3/8" from the top layer of the winding. The surface of the target is coated with a black thermal coating (emissivity = 0.97) for proper thermal imaging and a Fluke TI20 camera is used to capture the thermal images of the target. The thermal images obtained are shown in Fig. 12 and Fig. 13 and the temperature profiles are compared in Fig. 14 along the center horizontal guide lines (x-dimension) shown in the thermal images. Figure 12 (a) and (b) shows the non-uniform heating on the target when only A or B phase is individually excited. Figure 15 shows that there is minimal cross coupling of the phase currents because two different resonant frequencies are used for each of the two phases. The pattern has a periodicity of $2kx$ and is shifted by 180° in space as expected due to the flux density pattern of the individual phases. Figure 12 (c) shows the uniform heating along the surface of the target when both the phases are excited together. Fringing effects of the magnetic field at the

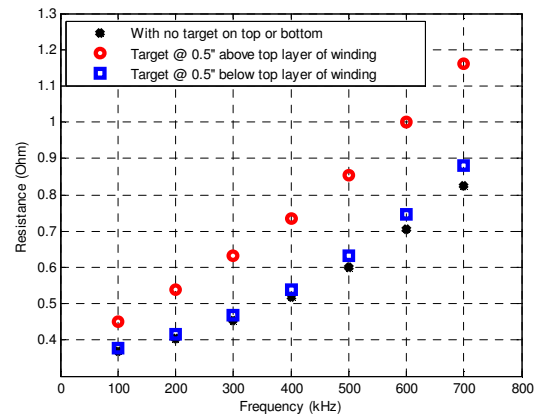


Figure 11. Measurement data from impedance analyzer: Change in resistance when a target is placed above the top layer winding is significantly higher compared to the change when the target is placed at same distance below.

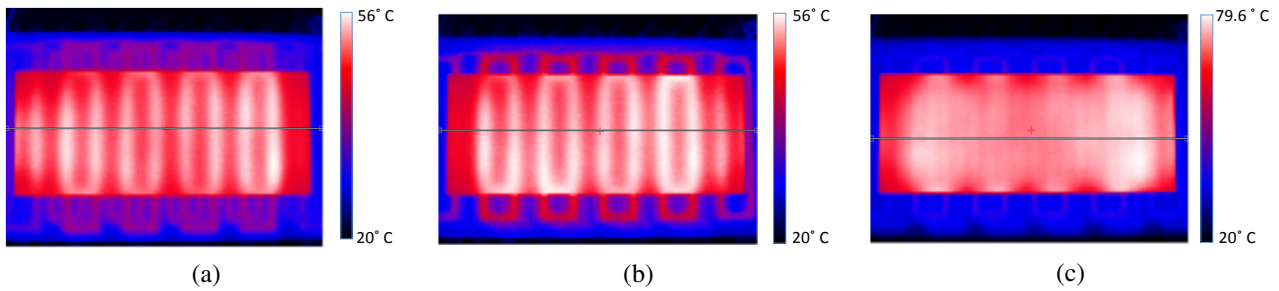


Figure 12. Thermal image of the steel target when placed at 3/8 inch above the top layer of the prototype. (a) Only A-phase is excited – input power = 38 W. (b) Only B-phase is excited – input power = 37.3 W (c) Both phases are excited – input power Phase A=38.2 W & phase B = 37.8 W.

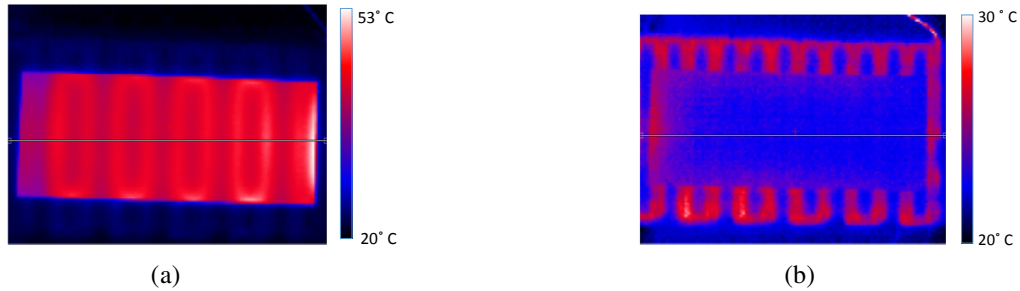


Figure 13. Thermal image of an additional steel target when placed at 0.4" below the top layer of the prototype with Phase A excitation. (a) With bottom layer of the winding disconnected. Resonant frequency adjusted to 349 kHz input power = 44.2 W. (b) With top and bottom winding layer connected input power = 44.7 W.

end of the windings cause in non-uniform heating at the edges.

With uniform heating obtained on top, another identical target is then placed on the back of the winding at a distance 0.4 inch from the top winding layer to evaluate the directionality of the heating. The A-phase is first excited with a disconnected bottom layer. As the inductance of the winding changes due to the removal of bottom layer connection, the resonant frequency is adjusted so that the A-phase still resonates with 20 nF. An average temperature rise of 45° C, shown in Fig. 14, is observed on the bottom target while the

thermal profile is similar to the top because of single phase excitation as shown in Fig. 13(a). Re-connecting the bottom layer results in no heating of the bottom target as shown in thermal image of Fig. 13(b) as well as on the temperature profile in Fig.14. The thermal image only shows heating up of the winding relative to the bottom target. This validates that the optimized winding behaves as a Halbach array providing both single side and uniform heating.

V. CONCLUSION

This paper demonstrates an approach for induction heating

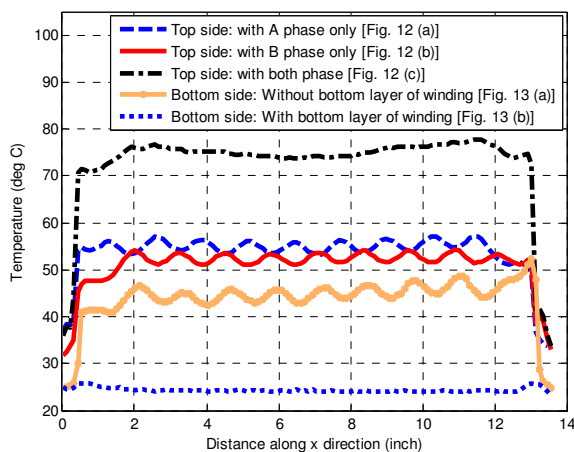


Figure 14. Temperature profiles along the center lines drawn on the thermal images of Fig. 12 and Fig. 13. While uniform heating is obtained on the top, no heating is produced on the bottom of the fully functional winding structure.

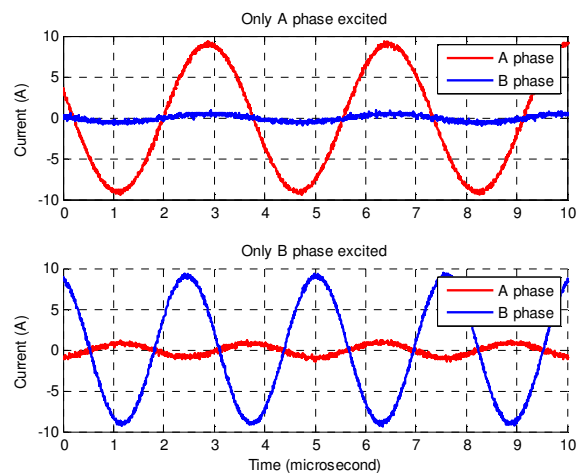


Figure 15. Measured current of the A phase and the B phase when excited individually. Tuning the phases at different resonant frequencies minimizes the cross coupling of the phases enabling independent excitation possible of the two phases.

by using uniform, single-sided magnetic fields, which is enabled by using multiple phases operating at multiple frequencies. The concept overcomes several shortcomings in traditional designs, including stray magnetic fields below the winding and non-uniform heating without requiring ferrites or other types of magnetic shielding. A design methodology for more efficient and lower cost windings for single-sided fields was also developed along with basic theoretical analysis and validation through simulation and experiments. The concept generalizes to other geometries and applications, extending the application space from consumer cooktops to chargers and non-contact power sources for transportation, industrial, and medical applications.

ACKNOWLEDGEMENT

This research was supported by The Grainger Foundation and the MIT EECS SuperUROP program. The authors wish to thank Prof. James L. Kirtley Jr. and Jorge Elizondo Martinez for their help and advice.

REFERENCES

- [1] V. Rudnev, *Handbook of induction heating*, New York: Marcel Dekker, 2003
- [2] J. R. Oleson, "A review of magnetic induction methods for hyperthermia treatment of cancer," *IEEE Trans Biomed Eng*, vol. 31, no. 1, pp. 91-7, Jan, 1984
- [3] P. R. Stauffer, P. K. Sneed, H. Hashemi, and T. L. Phillips, "Practical induction heating coil designs for clinical hyperthermia with ferromagnetic implants," *IEEE Trans Biomed Eng*, vol. 41, no. 1, pp. 17-28, Jan, 1994
- [4] Moreland, W.C., "The Induction Range: Its Performance and Its Development Problems," *Industry Applications*, IEEE Transactions on , vol.IA-9, no.1, pp.81,85, Jan. 1973
- [5] Acero, J.; Burdio, J. M.; Barragán, L.A.; Navarro, D.; Alonso, R.; Garcia, J.R.; Monterde, F.; Hernandez, P.; Llorente, S.; Garde, I., "The domestic induction heating appliance: An overview of recent research." *Applied Power Electronics Conference and Exposition, 2008. APEC 2008. Twenty-Third Annual IEEE* , vol., no., pp.651,657, 24-28 Feb. 2008
- [6] Souley, M.; Caux, S.; Pateau, O.; Maussion, P.; Lefevre, Y., "Optimization of the settings of multiphase induction heating system," *Industry Applications Society Annual Meeting (IAS), 2012 IEEE* , vol., no., pp.1,6, 7-11 Oct. 2012
- [7] Acero, J.; Alonso, R.; Burdio, J.-M.; Barragán, L.A., "Enhancement of induction heating performance by sandwiched planar windings," *Electronics Letters* , vol.42, no.4, pp.241,242, 16 Feb. 2006
- [8] Sergeant, P.L.; Dupre, L.R.; De Wulf, M.; Melkebeek, J. A A, "Optimizing active and passive magnetic shields in induction heating by a genetic algorithm," *Magnetics*, IEEE Transactions on , vol.39, no.6, pp.3486,3496, Nov. 2003
- [9] Ha Ngoc Pham; Fujita, H.; Ozaki, K.; Uchida, N., "Dynamic Analysis and Control for Resonant Currents in a Zone-Control Induction Heating System," *Power Electronics*, IEEE Transactions on , vol.28, no.3, pp.1297,1307, March 2013
- [10] Lucia, O.; Maussion, P.; Dede, E.J.; Burdio, J.M., "Induction Heating Technology and Its Applications: Past Developments, Current Technology, and Future Challenges," *Industrial Electronics*, IEEE Transactions on , vol.61, no.5, pp.2509,2520, May 2014
- [11] Al-Thaddeus Avestruz, Arthur H. Chang, Shahriar Khushrushahi, Arijit Banerjee, Steven B. Leeb, "Single-Sided AC Magnetic Fields For Induction Heating," presented at IECON 2013, Vienna, Austria
- [12] Dwari, S.; Parsa, L., "Design of Halbach-Array-Based Permanent-Magnet Motors With High Acceleration," *Industrial Electronics*, IEEE Transactions on , vol.58, no.9, pp.3768,3775, Sept. 2011
- [13] Mallinson, J.C., "One-sided fluxes -- A magnetic curiosity?," *Magnetics*, IEEE Transactions on , vol.9, no.4, pp.678,682, Dec 1973